AGU PUBLICATIONS

JGR

Journal of Geophysical Research: Atmospheres

RESEARCH ARTICLE
10.1002/2017JD027278

Key Points:
- The GEOS-Chem model reproduces ozone daytime deposition velocities observed at a suite of sites around the world to within a factor of 1.4
- Correct representation of land type is a key factor in reducing model biases
- Model biases in dry deposition velocity can impact surface concentrations of ozone by up to 4 ppb

Supporting Information:
- Supporting Information S1

Correspondence to:
S. J. Silva,
samsilva@mit.edu

Citation:
Silva, S. J., & Heald, C. L. (2018). Investigating dry deposition of ozone to vegetation. *Journal of Geophysical Research: Atmospheres*, *123*. https://doi.org/10.1002/2017JD027278

Received 9 JUN 2017
Accepted 3 DEC 2017
Accepted article online 12 DEC 2017

Investigating Dry Deposition of Ozone to Vegetation

Sam J. Silva[1] and **Colette L. Heald**[1]

[1]Department of Civil and Environmental Engineering, Massachusetts Institute of Technology, Cambridge, MA, USA

Abstract Atmospheric ozone loss through dry deposition to vegetation is a critically important process for both air quality and ecosystem health. The majority of atmospheric chemistry models calculate dry deposition using a resistance-in-series parameterization by Wesely (1989), which is dependent on many environmental variables and lookup table values. The uncertainties contained within this parameterization have not been fully explored, ultimately challenging our ability to understand global scale biosphere-atmosphere interactions. In this work, we evaluate the GEOS-Chem model simulation of ozone dry deposition using a globally distributed suite of observations. We find that simulated daytime deposition velocities generally reproduce the magnitude of observations to within a factor of 1.4. When correctly accounting for differences in land class between the observations and model, these biases improve, most substantially over the grasses and shrubs land class. These biases do not impact the global ozone burden substantially; however, they do lead to local absolute changes of up to 4 ppbv and relative changes of 15% in summer surface concentrations. We use MERRA meteorology from 1979 to 2008 to assess that the interannual variability in simulated annual mean ozone dry deposition due to model input meteorology is small (generally less than 5% over vegetated surfaces). Sensitivity experiments indicate that the simulation is most sensitive to the stomatal and ground surface resistances, as well as leaf area index. To improve ozone dry deposition models, more measurements are necessary over rainforests and various crop types, alongside constraints on individual depositional pathways and other in-canopy ozone loss processes.

1. Introduction

Dry deposition is a process by which aerosols and gases are removed from the atmosphere and taken up by the Earth's surface. It varies substantially across land types and ecosystems and is most prominent over vegetation (Wesely, 1989). There, it is an important loss mechanism for many atmospheric pollutants and climate forcers, particularly those that are highly biologically reactive such as ozone. Previous work has estimated that dry deposition is responsible for nearly 25% of all tropospheric ozone loss (Lelieveld & Dentener, 2000). A recent study of trends in ozone found that proper consideration of dry deposition is critical to the simulation of ozone extremes (Lin et al., 2017). Due to the substantial role that ozone plays in tropospheric chemistry as a greenhouse gas, a key oxidant, and a toxic surface pollutant, ozone loss through dry deposition is critically important to understand.

Dry deposition is highly dependent on turbulent transport, interfacial chemistry, and plant physiology (Wesely & Hicks, 2000). Due to the vast environmental complexities in these processes, alongside a relative dearth of measurements, models must rely on simplified parameterizations. The majority of modern chemical transport models calculate dry deposition using a resistor-in-series parameterization outlined in Wesely (1989) (hereafter referred to as W89). In this parameterization, the dry deposition flux of a gas is calculated following:

$$F = -V_d C$$

where F is the total flux out of the atmosphere; V_d is a transfer velocity, known as the "dry deposition velocity"; and C is the chemical concentration in the air. V_d is then calculated using a resistor in series approach:

$$V_d = (R_a + R_b + R_c)^{-1}$$

where R_a, R_b, and R_c represent the aerodynamic, boundary layer, and surface resistances, respectively. R_a and R_b are reasonably well defined; are largely dependent on turbulence, large-scale dynamics, and molecular diffusion; and are both typically more important during highly stable nocturnal conditions. The surface resistance, R_c is more important during the day. Uncertainties related to surface processes become substantially more influential in the calculation of R_c, making it the dominant focus of the majority of dry deposition-

related model development (Wesely & Hicks, 2000). The W89 algorithm for the calculation of R_c contains four depositional pathways that are calculated as individual resistances, and then summed in parallel. These are stomatal, cuticular, lower canopy, and ground surface. They are all calculated on a per land-type basis through a combination of initial lookup table values and physical dependencies. The plant response in W89 is determined through what is known as a "meteorological approach" (Niyogi et al., 1998), as opposed to direct simulation of plant physiology. The meteorological approach offers a substantially reduced computational time but likely does a poor job estimating the magnitude of dry deposition, relative to explicit simulation of plant physiology, during times of low photosynthesis (e.g., winter or at night) and does not account for second-order feedbacks (e.g., ozone plant damage) (Niyogi et al., 1998). The W89 algorithm was originally designed for use over land types in the northern midlatitudes and has since been substantially expanded and modified for use in global models (e.g., Wang et al., 1998; Zhang et al., 2003). Many of these modifications were derived from local data from a single field study (e.g., Jacob & Wofsy, 1990) and have yet to be fully tested against all available observations. Though parameterizations similar to W89 have been evaluated to some extent against observations at various field sites (e.g., Zhang et al., 2003), there are few large-scale evaluations. Hardacre et al. (2015) presented the first global scale evaluation of ozone dry deposition, comparing simulated monthly dry deposition across 15 chemistry-climate models with a variety of observations. They found biases as large as a factor of two, which they partially attribute to simulated land cover, and they stress the need for more detailed diagnostics of ozone dry deposition. Schwede et al. (2011) compared several dry deposition model schemes at the same location and found that, for ozone dry deposition, the simulated nonstomatal components of the surface resistance (R_c) contribute the most to disagreement across models. Importantly, there remain substantial uncertainties as to the abilities of these parameterizations to reproduce observed dry deposition velocities for ozone over poorly sampled land classes (Wesely & Hicks, 2000).

In this work, we use a suite of observations alongside the GEOS-Chem model to assess and constrain the dry deposition of ozone ($V_{d,O3}$) across the globe. We expand upon previous work by assessing current modeling efforts at high temporal resolution, across a wide variety of land types. We explore the net impacts on global air quality related to model uncertainty and bias and form a series of recommendations for model improvements and experimental constraints.

2. Model Description

We use the GEOS-Chem v9-02 chemical transport model (www.geos-chem.org) to simulate dry deposition and its impacts on a global scale. GEOS-Chem is a global 3-D model driven by assimilated meteorology from Global Modeling and Assimilation Office. Here we use meteorology from both the NASA GEOS-5 (2006) and MERRA products (1979–2008), at 2° × 2.5° resolution. The model includes an extensive HO_x-NO_x-VOC-O_3-BrO_x chemical mechanism (Mao et al., 2013) that has been used in several recent studies to better understand tropospheric ozone (e.g., Mao et al., 2013; Parrella et al., 2012; Travis et al., 2016). Global anthropogenic emissions are driven by the Emissions Database for Global Atmospheric Research version 3, and emissions from biomass burning are from the Global Fire Emissions Database (van der Werf et al., 2010).

Surface-atmosphere exchange processes in the model are driven by an updated land module developed by Geddes et al. (2016), which harmonizes the model description of several land-atmosphere exchange processes, including biogenic emissions and dry deposition. Dry deposition is calculated on a per land-type basis, with 11 total depositional land types: coniferous, deciduous, rainforest, grasses and shrubs, crops, arctic grass, water, glacier, bare, wetland, and urban. The land class distribution used is from the year 2000 inputs to the Community Land Model v.4 (http://www.cgd.ucar.edu/tss/clm), which was derived using satellite observations (Lawrence et al., 2011). This land distribution is described by 16 plant functional types, which are mapped to the 11 depositional land types within the W89 scheme. A similar model configuration has previously been used to study the air quality impacts of land use change (Geddes et al., 2016; Heald & Geddes, 2016; Silva et al., 2016).

3. Simulation of Dry Deposition

Within GEOS-Chem, dry deposition is calculated using a slightly modified version of the W89 algorithm for the calculation of R_c, including changes to adapt the original algorithm to the global scale (supporting

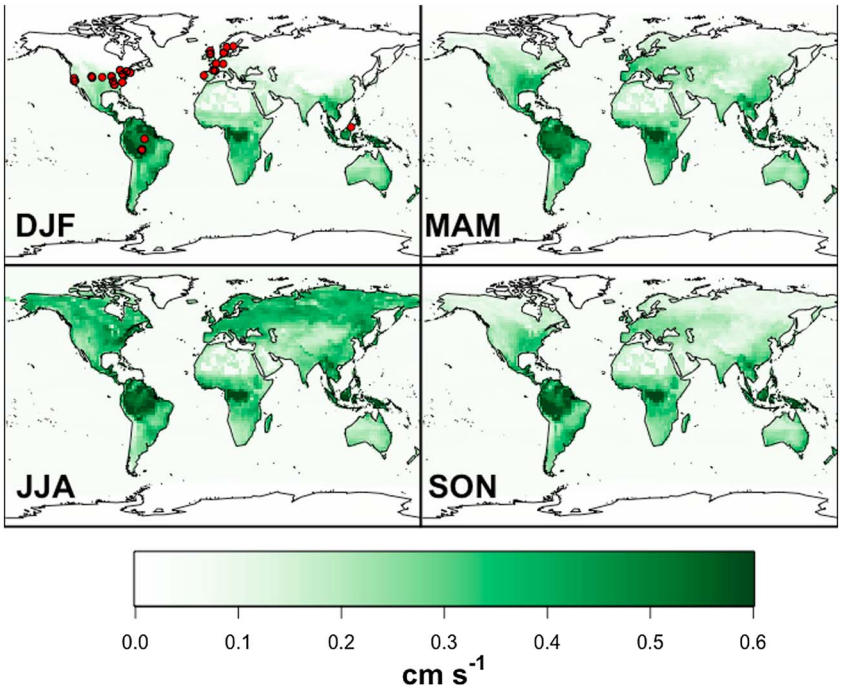

Figure 1. Seasonal mean $V_{d,O3}$ simulated by the GEOS-Chem model with the Wesely (1989) parameterization. The locations of observations are shown in the first panel.

information S1, Bey et al., 2001). Mainly, the lookup table values were modified across the various global land classes, including an additional tropical rainforest land class that was added following field work by Jacob and Wofsy (1990). These initial lookup table values do not vary seasonally as in W89; seasonality is instead captured as a function of varying surface luding leaf area index (LAI). Several additional changes to the resistance calculations were added, including changing the initial cuticular lookup table values to be on a per LAI basis, allowing for more consistent seasonality in this implementation. The dependence of the W89 algorithm on irradiance was also modified following Wang et al. (1998) to better account for canopy radiative transfer processes and the resulting changes in stomatal resistance. Importantly, the dry deposition algorithm as implemented in the GEOS-Chem model does not contain several measured processes known to influence dry deposition, including: the impact of wetted leaf surfaces, in-canopy chemical production and loss, stomatal damage, or a direct dependence on vapor pressure deficit (Emberson et al., 2013; Kavassalis & Murphy, 2017; Sadiq et al., 2017; Zhou et al., 2017).

The dry deposition scheme within GEOS-Chem produces $V_{d,O3}$ that are generally consistent with many other chemical transport models, with annual mean values all well within the ranges reported by Hardacre et al. (2015). Seasonal average global maps of $V_{d,O3}$ for the year 2006 are shown in Figure 1. Figure 1 illustrates the broad prominence of deposition across vegetated land classes, particularly the tropics. The northern boreal forests exhibit the response of this dry deposition scheme to the local seasonal cycles of vegetation. The ozone dry deposition flux can be calculated from the spatiotemporal distribution of both $V_{d,O3}$ and the surface concentrations of ozone. Table 1 displays the fraction of global annual ozone deposition flux alongside the fraction of the globe occupied by a given land class and the average $V_{d,O3}$, for a model simulation of the year 2006. The total simulated ozone deposition flux (896 Tg yr^{-1}), as well as the flux partitioning, is consistent with other studies (Hardacre et al., 2015), with nearly half (48.5%) of all ozone depositing onto vegetated land types and more than one-third (35%) depositing to the ocean as previously shown by Ganzeveld et al. (2009). While $V_{d,O3}$ to oceans is low (Figure 1), the extensive spatial coverage of the ocean makes it a nonnegligible fraction of tropospheric ozone loss. Recent work has suggested that the total amount of ozone depositing to the ocean is substantially lower than 35% (Luhar et al., 2016), related to the oversimplified parameterization of deposition to oceans commonly used in models. A reduction in oceanic $V_{d,O3}$ would further increase the prominence of vegetation.

Table 1
The Percent of Global Ozone Deposition Flux Simulated by GEOS-Chem Alongside the Percent of Global Surface Per Land Class and the Annual Mean Simulated $V_{d,O3}$

Land class	Coniferous	Deciduous	Rainforest	Grass	Crops	Water	Other
Percent of ozone Deposition flux	7.3	8.9	6.9	16.9	8.5	35.0	16.5
Percent of global Surface area	2.8	3.2	2.3	6.7	2.9	71.1	10.9
Mean ozone deposition Velocity (cm s^{-1})	0.16	0.23	0.38	0.20	0.24	0.04	0.10

Note. The "other" category includes desert, wetlands, urban, ice, and tundra.

4. Observations

To test our simulated dry deposition, we compiled a suite of globally distributed observations, summarized in Table 2 (see supporting information S2 for more details). These measurements were made using the eddy covariance or flux gradient methods (e.g., Mikkelsen et al., 2000; Muller et al., 2010) and report data on time scales ranging from hourly to monthly. We use here only direct measurements of $V_{d,O3}$ rather than derived values. For observation-model comparisons, we extracted all available data from these studies, for a total of 78 data sets. These data cover the top five major vegetated land classes used within the GEOS-Chem model framework for dry deposition (Table 1), and their locations are shown on Figure 1. To our knowledge, this is the largest set of direct observations of $V_{d,O3}$ compiled for model assessment. Despite this, the data set is not large enough to further disaggregate regional or species-specific uptake of vegetation. Furthermore, we note that the observations preferentially sample North America and Europe. The mean observed ozone deposition velocities vary from 0.27 cm s^{-1} over coniferous forests to 0.61 cm s^{-1} over tropical rainforests. The overall range within each land class is fairly substantial, with minimum values typically near zero and maximum values typically near 1.5 cm s^{-1}. $V_{d,O3}$ can exceed 2 cm s^{-1} over the rainforest; this is consistent across several field studies in the Amazon (Fan et al., 1990; Rummel et al., 2007). The observed minimums of less than zero generally come from few (less than 10) individual observations per land class and occur at night, likely due to challenges observing ozone fluxes during highly stable nocturnal conditions. In general, uncertainties in both eddy covariance and flux gradient approaches range from 10 to 20% throughout the day (Mikkelsen et al., 2000; Muller et al., 2010).

As shown in Table 2, there are substantially fewer sets of data over rainforests ($n = 5$), including none during local winter, which could lead to challenges in constraining dry deposition across that land class. Over all land classes, observations are biased to the growing season months (spring, summer, and fall). This limits our ability to evaluate the parameterization during local winters. However, given that the majority of dry deposition

Table 2
Summary of Observations Used in This Work

Land type	Mean (cm s^{-1})	Range (cm s^{-1})	Available seasons	Number of data sets	Reference (hourly/daily/monthly)
Coniferous	0.27	(−0.07, 1.39)	Summer, fall, winter, spring	25	Coe et al. (1995) (d), Finkelstein et al. (2000) (h), Granat and Richter (1995) (h), Hole et al. (2004) (h/d), Kumar et al. (2011) (h), Kurpius et al. (2002) (h/d), Lamaud et al. (1994) (h), Mikkelsen et al. (2004) (h), Munger et al. (1996) (h), Park et al. (2014) (h), Turnipseed et al. (2009) (h)
Deciduous	0.42	(0.01, 1.60)	Summer, fall, winter, spring	20	Finkelstein et al. (2000) (h/d), Mikkelsen et al. (2000) (h/d/m), Munger et al. (1996) (h), Padro et al. (1991) (h/d), Padro et al. (1992) (h/d), Wu et al. (2011) (h/d), Zhang et al. (2002) (h)
Rainforest	0.61	(−0.04, 2.65)	Summer, fall, spring	5	Fan et al. (1990) (h), Fowler et al. (2011) (h), Rummel et al. (2007) (h)
Grass	0.32	(0.01, 1.24)	Summer, fall, winter, spring	11	Droppo (1985) (h), Fowler et al. (2001) (h), Gao and Wesely (1995) (d), Padro et al. (1994) (h), Pio et al. (2000) (h)
Crops	0.33	(−0.11, 1.0)	Summer, fall, winter, spring	14	Coyle et al. (2009) (h), Meyers et al. (1998) (h), Padro et al. (1994) (h), Pilegaard et al. (1998) (h), Sigler et al. (2002) (h), Stella et al. (2011) (h), Zhang et al. (2002) (h)

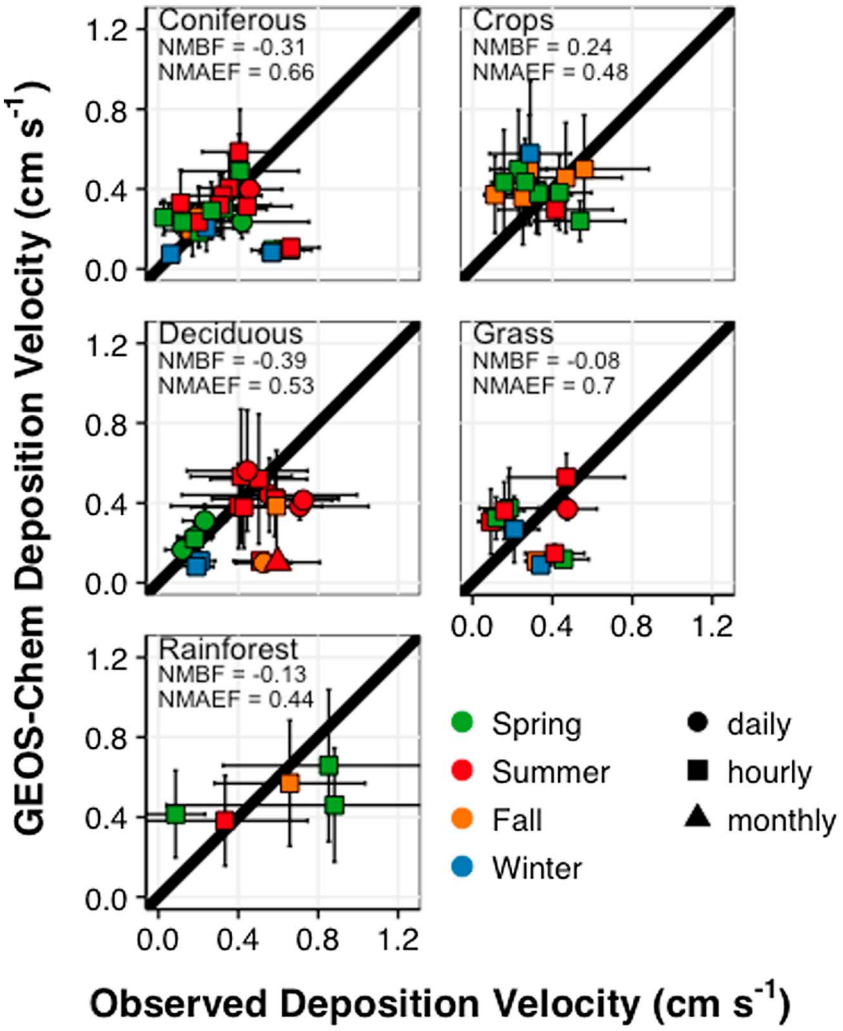

Figure 2. Simulated versus observed mean $V_{d,O3}$ velocities for five major land classes. The bars on each data point represent ±1 standard deviation. The 1-to-1 line is shown in black. The colors indicate season, and the shape of the points indicates the temporal resolution of the measurements.

occurs during the growing season, this is not likely a substantial limitation. The most data are available over the coniferous (n = 25) and deciduous forests (n = 21), and there are a modest number of data sets over crops (n = 14) and grasses and shrubs (n = 11). Within the GEOS-Chem model, all plant species are lumped into these five broad categories. This is a clear simplification and is particularly important over the crop land class. Given the potentially large differences in plant phenology and management practices of different crops, including stress response and photosynthetic pathways (C3 versus C4), this model land-type aggregation likely misses some key characteristics of deposition and may lead to inconsistencies across the 14 separate data sets over the "crops" land class.

5. Evaluation of the Model Simulation of $V_{d,O3}$

We evaluate model simulated $V_{d,O3}$ in a stepwise manner to be consistent with previous work (e.g., Hardacre et al., 2015; Travis et al., 2016). We initially assess the base version of the model for an arbitrary year, followed by tests involving changes to both land classification and input meteorology. Model simulated $V_{d,O3}$ for the meteorological year 2006 was sampled to each of the observations at a matching time resolution, up to a per-hour basis. The mean comparisons across land classes are shown in Figure 2, where averages across each data set are compared with averages of the simulated $V_{d,O3}$. The colors in Figure 2 correspond to the dominant

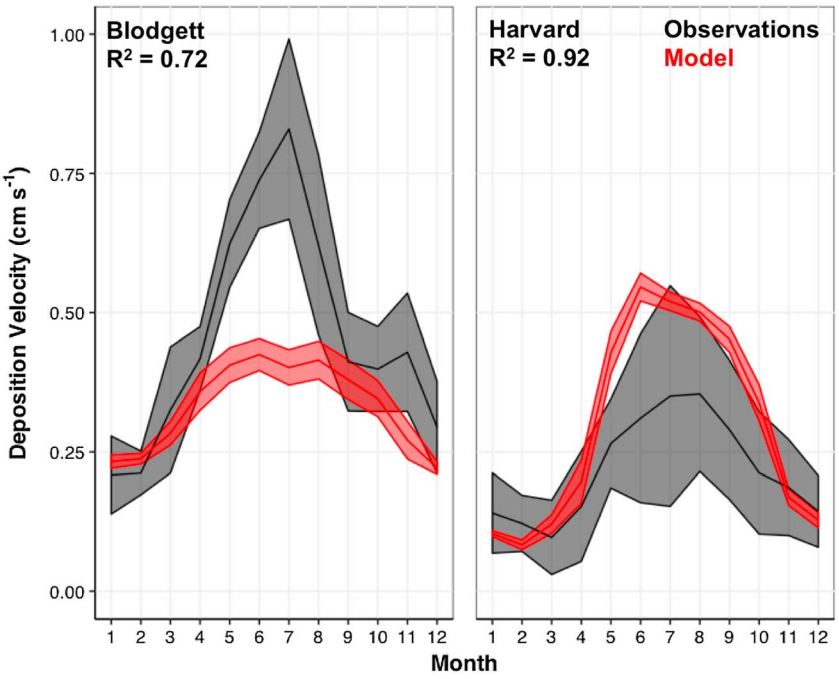

Figure 3. Simulated versus observed monthly mean $V_{d,O3}$ over Harvard and Blodgett Forest. The envelopes show the standard deviation of observed and simulated monthly mean deposition velocities, centered on the mean values.

season in which the measurements were taken, and the shapes represent the time resolution of the data. To evaluate the model simulation we use the normalized mean bias factor (NMBF) and normalized mean absolute error factor (NMAEF) formulation outlined in Yu et al. (2006). NMBF and NMAEF values closer to zero indicate better agreement between the data and model. If the NMBF is positive, the model overestimates the observations by a factor of 1 + NMBF. If the NMBF is negative, the model underestimates the observations by a factor of 1 − NMBF. A NMAEF of 1 indicates that the absolute gross error between the data and model is on the same order as the mean observation (model) value for overprediction (underprediction).

In general, the model reproduces the mean observed $V_{d,O3}$ to the correct order of magnitude, and there is no substantial disagreement with the observations as a function of either season or observational time resolution. However, a low overall combined R^2 (0.04) across all the data suggests a lack of model skill in reproducing the spatial variation in mean $V_{d,O3}$. The NMBF across land classes is within ±0.4 and generally negative (summarized in Figure 2), indicating that the model average underestimates the observational average within a factor of 1.4. The exception to this is over the crops land class, where the model overestimates mean observed ozone deposition velocities with an NMBF of 0.24. The NMAEF for each land class ranges from 0.44 to 0.7 (Figure 2), which is consistent with the relatively large absolute gross error between the model and bulk observations. These results agree with the monthly average comparisons reported in Hardacre et al. (2015), where they found differences between observed and simulated $V_{d,O3}$ within a factor of 2.

In addition to evaluating the model bias across the mean observations, we explore the model skill in reproducing the temporal variability of measured $V_{d,O3}$. To compare with Hardacre et al. (2015), we first evaluate our simulation against monthly average $V_{d,O3}$ reported at available CASTNET sites across North America (https://www.epa.gov/castnet) and find a similarly high R^2 (median $>$ 0.7), suggesting that the model captures the seasonal cycle of monthly average $V_{d,O3}$. It is important to note that CASTNET dry deposition velocities are not observed but instead derived using the multilayer model (Wu et al., 2003). We therefore focus our analysis on the direct measurements of dry deposition velocities from the available literature outlined in section 4. Figure 3 shows that the model also captures the seasonal cycle at the two long-term eddy flux measurement sites when sampled to the correct time period and location, over Harvard (deciduous) and Blodgett (coniferous) Forests (R^2 of 0.92 and 0.72, respectively) (Fares et al., 2010, 2012; Munger & Wofsy, 1999a). The

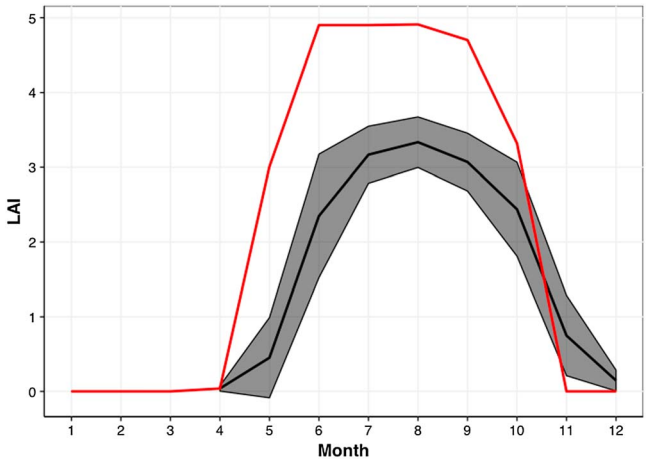

Figure 4. Simulated versus observed deciduous LAI at Harvard Forest. The envelope on the observations shows the standard deviation of monthly mean LAI from 1998 to 2005, centered on the mean values. There is no interannual variation in the model LAI.

NMBF and NMAEF over the Blodgett Forest site are −0.38 and 0.44, respectively. While the cause of the model underestimation during summer months at Blodgett Forest cannot be explained from the available observations, the NMBF and NMAEF are consistent with other coniferous forest sites (see Figure 2). The NMAEF over the Harvard Forest site is 0.55, in line with the bulk deciduous forests comparisons; however, the Harvard Forest NMBF is 0.38, the opposite sign from the bulk comparisons. This indicates that the model generally overestimates the observations by a factor of 1.38 at the Harvard Forest site. Consistent with the analysis by Clifton et al. (2016), we find that the overestimate is most apparent during the summer months (Figure 3); we suggest that this is likely related to the model overestimate of LAI during that time period. Comparisons between the simulated LAI and field survey-measured LAI of deciduous trees in Harvard Forest (Munger & Wofsy, 1999b) are shown in Figure 4. As simulated $V_{d,O3}$ is strongly dependent on LAI, the LAI bias (NMBF = 0.6) is likely to be a major factor contributing to the overestimation in $V_{d,O3}$. In addition, the model LAI increases 1 to 2 months earlier (in May–June) than the observations, which likely contributes to the prominent early springtime overestimate in $V_{d,O3}$ in the model.

The aggregation of the observations to the monthly time scale inflates much of the model skill in reproducing the observations. When the long-term direct observations of $V_{d,O3}$ are compared at the hourly temporal resolution, the R^2 values are much lower (0.05 for Harvard Forest and 0.29 for Blodgett Forest). Hourly CASTNET data similarly show very low values of R^2 (median $<$ 0.2). This further motivates an analysis at high temporal resolution. The data sets reported in Table 2 vary in time scales, with most data being reported hourly (n = 62), and far fewer reported daily across seasons (n = 12), and monthly (n = 1). These individual hourly comparisons of each individual data set generally have an R^2 value of ~0.6, which is consistent with the model capturing the broad diurnal changes in $V_{d,O3}$. The daily comparisons have a lower R^2 of ~0.25, with a substantial range from site to site (from R^2 = 0.002 in a Canadian deciduous forest to R^2 = 0.75 in a coniferous forest in Norway). This indicates that the model struggles to capture some of the day-to-day variability in $V_{d,O3}$ in many regions.

To further investigate the potential causes of the observed and modeled $V_{d,O3}$ disagreement, we focus our analysis on the data sets reporting on the hourly time scales (Figure 5), where we have the most available reported observations (n = 58), as compared to other time scales. The model captures the diurnal cycle across vegetation classes, with elevated deposition velocities during the midday relative to low nocturnal velocities. In general, these hourly comparisons are consistent with the bulk average comparisons of $V_{d,O3}$ previously discussed. The relative good agreement between the observed and modeled $V_{d,O3}$ over the coniferous forests is apparent from Figure 5, as well as the net overestimation over crops, and the net underestimation over the deciduous, grass, and rainforest land classes. The largest underestimation is over the grass land class. The large variability in the rainforest comparisons is apparent in Figure 5, which is at least partly due to the dearth of measurements.

From the hourly time series, it becomes apparent that the relative differences between the observations and the model vary as a function of time of day. This reflects changes in the importance of various processes and model skill in simulating those processes. During the day, deposition to vegetation is dominated by the surface resistance, largely through the stomatal pathway. In contrast, nocturnal deposition is typically controlled by the aerodynamic resistance, as atmospheric stability increases at night. The nocturnal biases are larger than those during the day for all land classes except grasses. The NMBFs between the hours of 8 a.m. and 8 p.m. are generally within ±0.3 for all but the grass land type and are generally higher (within ±0.45) during the night. The NMAEFs over the forested land classes are much larger ($>$0.75) nocturnally than during the day ($<$0.75) but are consistent across the crops (0.5) and grass (1.5) land classes, indicative of wider nocturnal spread over forests. Though the nocturnal biases and data-model spread are larger, the magnitude of $V_{d,O3}$ at night is rather low and thus not a major loss pathway of O_3. Similar to the bulk comparisons, most of the observations available at hourly time scales were made during the local growing season. This limits

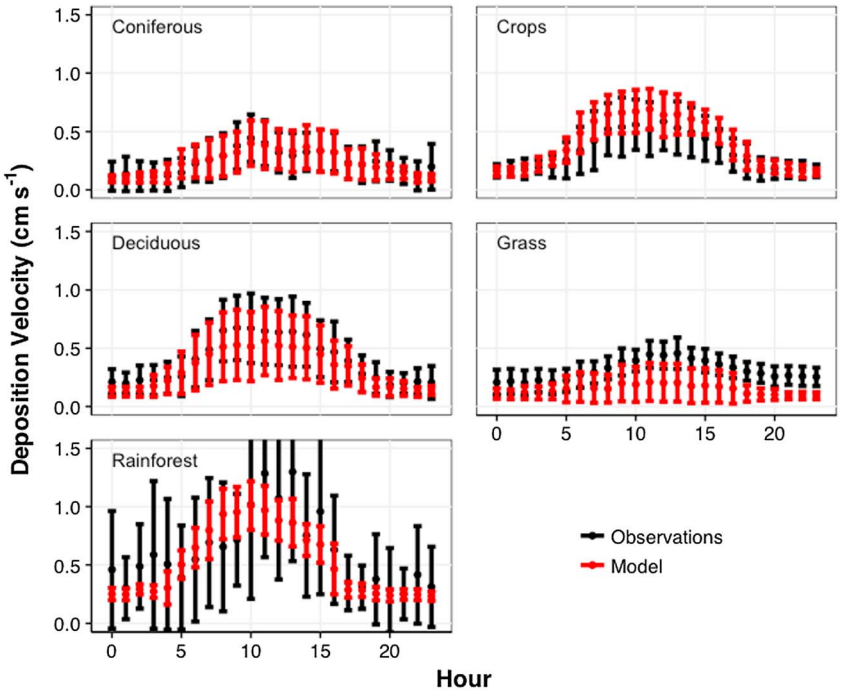

Figure 5. Hourly simulated (red) and observed (black) $V_{d,O3}$ for five major land classes. The points represent the mean across the observational period, and the bars represent ±1 standard deviation.

our ability to assess the diurnal variability of the parameterization across seasons. The observational bias also contributes to the relatively wide spread between the observations and the model, as indicated by the large NMAEF.

There are two aspects that could confound the evaluation of simulated $V_{d,O3}$: land-type mismatch between the data and the model and the choice of a static meteorological year (2006). There is substantial disagreement between the model and certain observations related to the model land class representation. This is at least partially due to how the model produces a grid box average $V_{d,O3}$ accounting for all represented land classes, and observations are made at a specific location. This issue with land class representation explains some of the clusters of observations that are outliers in Figure 2. For example, the cluster of model-underestimated values over coniferous forests is associated with several data sets from Mikkelsen et al. (2000). These measurements were taken at a coastal site in Denmark, where the model represents the surrounding grid box as ~65% water. Since the deposition velocities of ozone over water are much lower than those over coniferous forests, the land class disagreement leads to the large underestimation in the model. To account for these land-type representation issues, we perform a sensitivity experiment where we force the model land class distribution to match the land class of the observations. This is achieved by scaling up the observed land classes to 100% of the grid box land fraction, including scaling other related surface parameters (LAI and surface roughness). Additionally, the comparisons thus far used a single year of meteorology for the evaluation. Given the dependence of the dry deposition parameterization on local meteorology, it may be important to match the model meteorology with that of the observations. To remedy the mismatch with meteorology, we simulated observed $V_{d,O3}$ using MERRA meteorological inputs from the same year that the observations were taken. We then compare the hourly time series of these two model scenarios along with the base model simulations and the observations, shown in Figure 6. The matched meteorology and land-type scenarios are labeled "Met-Fix" and "LT-Fix."

These sensitivity experiments provide new insight into the importance of representing land use and meteorology for simulating dry deposition. Changing the meteorology to the correct year (the "Met-Fix" simulation) has little impact on the simulation of $V_{d,O3}$. The Met-Fix values consistently overlap with those from the base simulation and do not show any notable improvements in the hourly time series comparisons of Figure 6. The

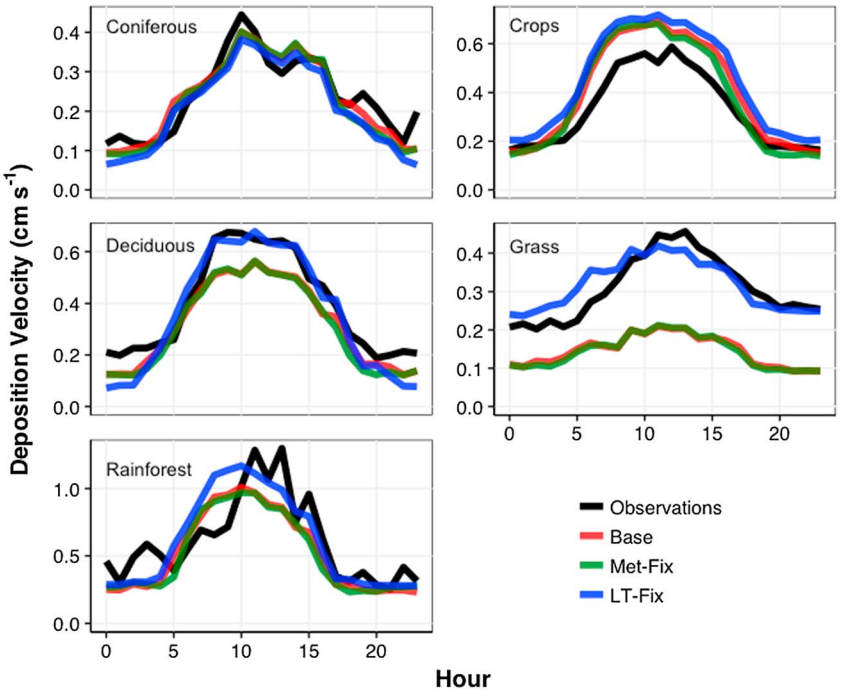

Figure 6. Mean hourly $V_{d,O3}$ across all three model scenarios and the observations for five major land classes. Observations and base are as shown in Figure 5, which shows the variability in these means. The base simulation uses 2006 GEOS-5 meteorology and the default GEOS-Chem land class distribution. The Met-Fix scenario uses the matching meteorological year to the measurements, and the LT-Fix scenarios force the simulated land type to agree with observations.

only exception is improved agreement with the observations during nocturnal deposition over crops. The average NMBF over this time period over crops decreases from 0.11 to 0.03. The lack of broad improvement from the Met-Fix simulation indicates that the choice of meteorological reanalysis year is not a strong driver of model disagreement with observations. Figure 7 reinforces this, where the ratio of the standard deviation to the annual mean $V_{d,O3}$ across 24 meteorological years (1979–2008) used in the Met-Fix simulations is shown. This figure gives a general sense of the variability in $V_{d,O3}$ associated with model meteorology, with a maximum of ~12%, and a value of less than ~5% over the majority of vegetated grid boxes. This suggests that the year-to-year changes in meteorology within the MERRA reanalysis product are not strong drivers of mean $V_{d,O3}$ variability, consistent with the Clifton et al. (2016) analysis at Harvard Forest. However, given the challenges in simulating stability and turbulent parameters, it is possible that biases or uncertainties persist throughout all model years of the MERRA product and that meteorological variability is underestimated.

In contrast with the small impact of meteorological changes, imposing land cover agreement in the model substantially improves the simulation of $V_{d,O3}$ in many classes. The most dramatic change is over the grass land class, where the LT-Fix simulation shows that the large model underestimation of deposition velocities is vastly improved when the corrected land classes are taken into consideration. This is related to the model subgrid distribution of grasses and shrubs where grasses and shrubs never make up more than 80% of a model grid box and often overlap with barren and water land classes where deposition velocities are low. The NMBF over grasses is reduced from less than −1.0 to within ±0.25 in the LT-Fix scenario. Accompanying the reduction in NMBF over grass is a large change in NMAEF, from greater than 1.25, to below 0.5. This is indicative of much better agreement between both the observed and modeled deposition velocities than the base comparisons would indicate. From this, we can conclude that the massive underestimation over grass and shrubs land class is not the result of a poorly parameterized model. The LT-Fix simulation also improves the simulation of daytime deposition velocities over deciduous and coniferous forests, though disagreement during the night is larger. This nocturnal disagreement is accompanied by large nocturnal increases in the NMAEF, from daytime values of 0.5 to nocturnal values of up to 2. This bias and

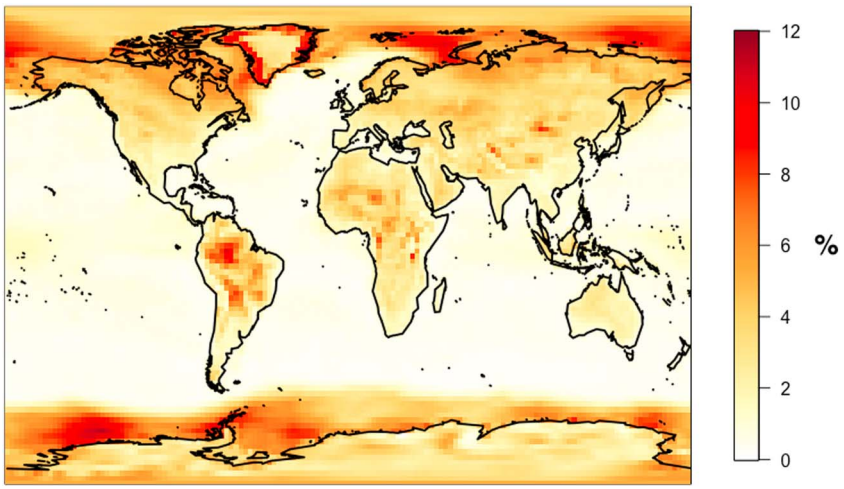

Figure 7. The ratio of the standard deviation to the annual mean $V_{d,O3}$ as a percent, shown across 24 meteorological years from 1979 to 2006. The base land map was kept constant throughout all simulations. High values at high latitudes are small in overall magnitude and related to changes in local meteorology and variation in snow cover.

spread demonstrates challenges in constraining nocturnal deposition velocities. This disagreement could be related to an underestimation of nonstomatal deposition (lower canopy, cuticular, or ground surface), or simply observational bias toward nonzero fluxes due to observational challenges during highly stable atmospheric conditions. Across the rainforest and crops land classes, the impact of the LT-Fix simulation is more muted. It offers minor improvements in the simulation over the rainforest and minor reductions in model skill over crops. The evaluation of the simulated $V_{d,O3}$ over both rainforests and crops is challenging in part due to the limited observational sampling available over these land classes. Though there are 14 total different references reporting data sets over crops, the wide variety in cropland influences on $V_{d,O3}$ (Wesely & Hicks, 2000) alongside the single crop type with the GEOS-Chem model strongly implies that representation issues may play a role in these comparisons. This underrepresentation is also present in the rainforest evaluation, where we only have three field campaigns reporting data.

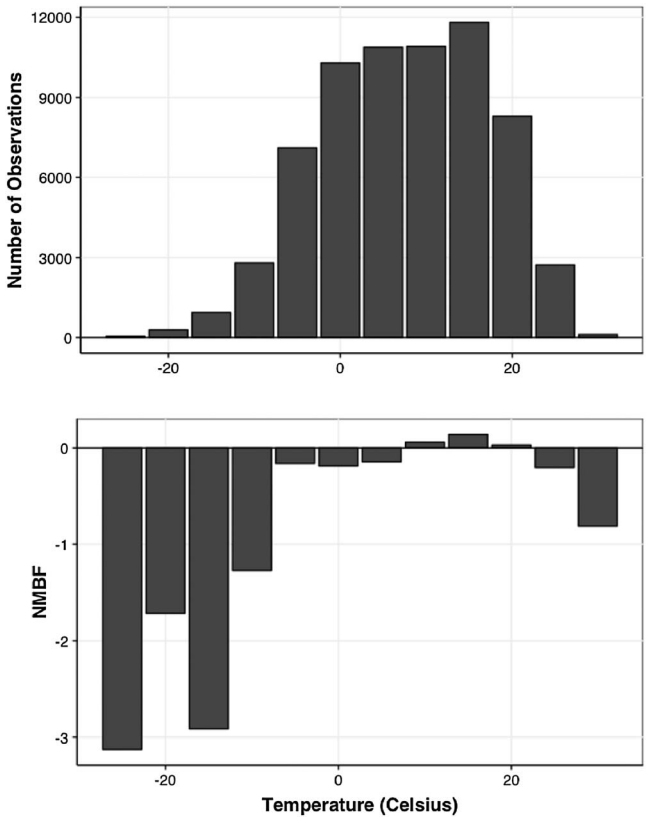

Figure 8. The number of observations and NMBF at the Harvard Forest and Blodgett Forest 438 locations as a function of observed temperature. Temperature bins are 5°C.

Several chemistry-climate models do not contain a specific parameterization for the rainforest land class, where, instead, the rainforest is considered to be a deciduous forest or something similar (Hardacre et al., 2015). Given the large uncertainty in the simulation of $V_{d,O3}$ over the rainforest related to the dearth of measurements, we perform a set of simulations to test the justification of including a separate rainforest land class. In these simulations, the parameterization of $V_{d,O3}$ over the rainforest land class is replaced with that of deciduous forests, while the LAI and roughness height of the rainforest land class are kept constant. When compared with observations, the simulation replacing rainforest with deciduous forests had a worse NMBF (by ~10%) and a slightly larger NMAEF than the base simulation. This suggests that inclusion of a separate rainforest land class is warranted, despite the large uncertainties.

There are two long-term data sets used in this work (Harvard and Blodgett Forest) that contain ancillary meteorological data (including photosynthetically active radiation, relative humidity, temperature, air pressure, and wind speeds) that could be used to evaluate the

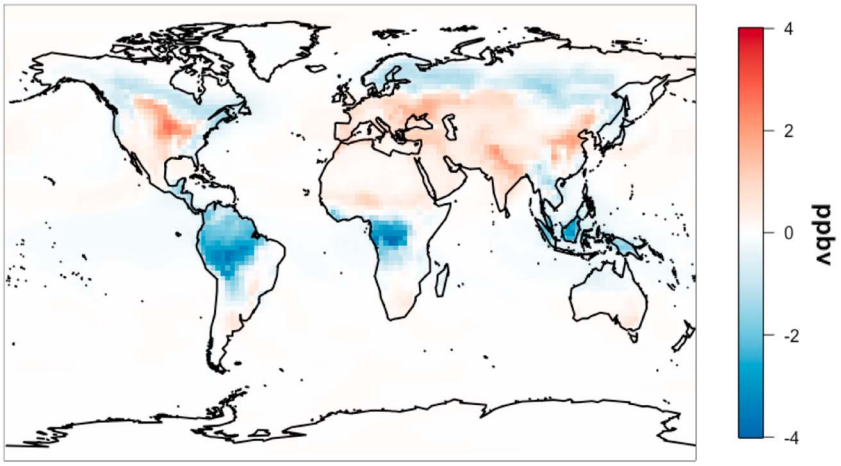

Figure 9. Mean summertime surface ozone difference between the base run and the simulation scaled to eliminate the model bias against observed $V_{d,O3}$ (scaled-base). Relative differences of surface ozone are as large as 15%.

parameterization currently used in the GEOS-Chem model (Munger & Wofsy, 1999a; Fares et al., 2010, 2012). Of the available ancillary data, temperature is the only variable for which there is a coherent bias in the response of the modeled $V_{d,O3}$ across both sites that is clearly linked to factors within the parameterization. Figure 8 shows the distribution of the observations and the NMBF of the model across 5°C temperature bins. A strong negative NMBF is apparent for temperatures below −7.5°C, where the model substantially underestimates the observations of $V_{d,O3}$ by more than a factor of 2. The W89 parameterization responds to temperature through two terms. The first term is the simulated closure of plant stomates at temperatures below 0°C by increasing the stomatal resistance to a very high number. This is reasonably consistent with observations and other dry deposition models (Zhang et al., 2003). The second term decreases the nonstomatal resistances through an exponential term that varies with surface temperature (T_s, °C), $1{,}000e^{(-Ts\ -\ 4)}$. This was intended to account for the reduced capacity for chemical ozone uptake by canopy and ground surfaces at cold temperatures but grows extremely large at low temperatures. To correct for this, we recommend setting a maximum for the exponential term ($1{,}000e^{(-Ts\ -\ 4)}$) at 5×10^5, consistent with the factor of 2 temperature limitation in the parameterization of Zhang et al. (2003).

6. Impact on the Simulation of Surface Ozone

Given the large variability in model $V_{d,O3}$ bias across time of day and land class, it is important to understand what potential impact these biases will have on model simulated surface ozone concentrations. To address this question, we scale modeled deposition velocities on an hourly per land class basis to match observations, according to the biases assessed from the model evaluation in section 5. We compare this simulation to a base run of the model without scaling, shown in Figure 9 for the northern hemispheric summer (JJA) months.

The global burden of ozone with this correction to $V_{d,O3}$ remains largely unchanged; however, local changes in surface concentrations may be substantial. There are three broad signatures associated with the bias scaling, each of which is evident in Figure 9. Over the northern boreal forest, correcting the small low bias in dry deposition over both coniferous and deciduous forests leads to a decrease in summer surface ozone of approximately 2 ppbv. Across the midlatitudes, there is a general increase in summer surface ozone of up to 3 ppbv. This is associated with the scaled croplands, where the simulated deposition velocities were too high. The reduction in ozone deposition velocities leads to a decrease in the local sink of ozone and thus an increase in concentrations. Finally, a large decrease in summer surface ozone over the tropical rainforests is due to increases in deposition velocities for both deciduous trees and the rainforest land classes. These tropical changes in surface ozone are the largest in relative terms (up to 15%) and regularly exceed 2 ppbv. These changes are substantial and move many midlatitude regions toward more unhealthy levels of ozone.

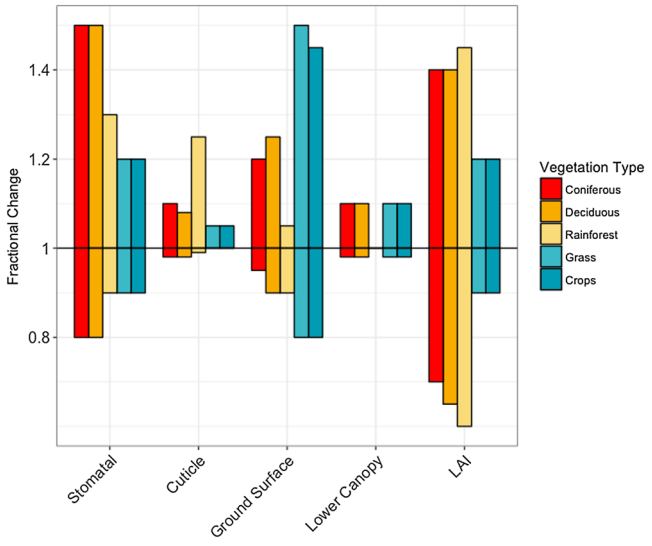

Figure 10. The fractional change in annual mean $V_{d,O3}$ in grid boxes dominated by a given land class due to a ±50% change in the resistance pathways and LAI.

The base model simulations of $V_{d,O3}$ over the coniferous and deciduous forests and crops are quite similar (Table 1); however, the bias-corrected simulations move them further apart. This has implications for land use change experiments (Heald & Geddes, 2016; Silva et al., 2016). The base model simulation used in previous studies suggests that the impact of historical land use change on the vegetative sink of ozone is small (Heald & Geddes, 2016), but this is likely underestimated. The larger difference between forests and crops shown here would ultimately lead to a substantial decrease in the local sink of ozone in a scenario considering a forest to cropland transition, which would then lead to an increase in ozone concentrations.

7. Uncertainty in Simulated $V_{d,O3}$

The above evaluation indicates that the GEOS-Chem model generally captures the magnitude of $V_{d,O3}$ at locations across the globe, but there remain gaps in model skill. In the broader context of the model uncertainty, it is likely that physical process missing from the model contributes to errors in simulated deposition velocities. For example, the nocturnal low bias (apparent in Figures 3 and 4) could be evidence of missing processes related to nonstomatal deposition. However, a systematic uncertainty analysis of the lookup table values and the individual model processes is not possible given that the reasonable range for a given parameter is not well known (W89). Therefore, to explore how the model parameterization might be improved, we performed a basic sensitivity study of the model parameterization of $V_{d,O3}$. Each of the four depositional pathways (stomatal, cuticular, lower canopy, and ground surface) as well as model LAI was modulated by ±50%, and the net impact on simulated annual mean ozone deposition velocities is shown in Figure 10.

In general, these perturbations are not symmetric about zero. This is related to the specifics of the parameterization, where each pathway is added in series. As an individual pathway R_i increases, the deposition velocity decreases, and the overall influence on the total deposition velocity of R_i decreases ($1/R_i -> 0$) relative to the influence of the other pathways. This is not the case when R_i decreases and the deposition velocity increases, as the upper bound on $1/R_i$ is infinite. Thus, fractional responses in $V_{d,O3}$ shown in Figure 10 are larger for positive perturbations. From Figure 10, it is apparent that there is a strong distinction between the model simulation of $V_{d,O3}$ over forested land classes versus grasses and crops. Deposition over the coniferous and deciduous land classes is strongly dependent on the stomatal resistance and secondarily on the ground surface resistance. Varying the stomatal resistances leads to changes in $V_{d,O3}$ by a factor of 0.8 to 1.5, over coniferous and deciduous forests, whereas the ground surface variability leads to changes by a factor of 0.9 to 1.2. Deposition over the grasses and crops land classes is the inverse, with a strong dependence on the ground surface resistance, followed by the stomatal resistance. The parameterization of the deposition over the rainforest land class is less sensitive to the stomatal and ground surface resistances than the other forested land classes but substantially more sensitive (up to a factor of 1.25) to the cuticular resistance pathway. Deposition over all land classes has little dependence on the lower canopy resistance, with the rainforest land class having near zero sensitivity to this resistance.

The additional LAI sensitivity in Figure 10 demonstrates the strong reliance of the $V_{d,O3}$ parameterization on this metric for biomass density. Since LAI is an important variable in the calculation of both stomatal and cuticular resistances, deposition velocities over the forested land classes scale nearly linearly with perturbations to LAI (factors of 0.65 to 1.4). However, the relative lack of importance of the stomatal and cuticular pathways within grasses and crop land classes leads to relatively smaller sensitivity to LAI changes (factors of 0.9 to 1.2). Varying LAI by up to 50% is consistent with the uncertainties in current global estimates. Fang et al. (2013) indicate that the available observed satellite estimates of LAI are broadly consistent with each other but have uncertainties ranging from ~10 to 115%. They find that these uncertainties vary substantially with retrieval methodology and across land classes, with the largest uncertainties over forested land classes and ecological transition areas.

8. Conclusions

In this work, we have evaluated a commonly used model parameterization for $V_{d,O3}$. Comparisons with observations show that daytime deposition velocities are generally within a factor of 1.25 for grasses, deciduous, and coniferous land classes and within a factor of 1.5 over crops and the rainforests land classes. These biases are substantially larger nocturnally, which could be related to issues in either simulated meteorology or the model parameterization. We also identify a low bias in the simulated $V_{d,O3}$ in cold conditions, which can be rectified by capping the temperature sensitivity in the W89 parameterization. These biases do not significantly impact the global ozone burden; however, they do lead to local absolute changes in surface ozone of up to ±4 ppbv and relative changes of up to 15%. Our evaluation indicates that while the W89 parameterization does capture the diurnal and seasonal cycle over vegetation, the spatial and day-to-day skill in the model is not high. This suggests that the W89 parameterization may not capture some of the leading sources of variability in ozone dry deposition.

Since the model parameterization contains many variables and is fit to observations, it is likely that there is at least some degree of model over fitting occurring. For example, the daytime agreement over forest does not suggest a large missing loss pathway associated with BVOC oxidation or other in-canopy chemistry-related processes; however, the current parameterization might compensate for this by overestimating another term. This over fitting is potentially responsible for the various shortcomings in the model evaluation, and the sensitivity tests point to how to best address these model shortcomings. Field measurements of individual resistance pathways, similar to Cape, Hamilton, and Heal (2009), would allow for improved constraints on the overall parameterization. In addition, complementary measurements of meteorological and phenological parameters, which, to date, are available with few dry deposition data sets, could enable a more process-based analysis. This is in contrast to the benefit of additional bulk $V_{d,O3}$ measurements during the growing season, which, given the complexity of the current parameterization, would likely lead only to improved uncertainty characterization. This, in part, explains our inability to distinguish if the lack of important model processes (such as stomatal damage from ozone) substantially reduces the overall model skill in simulating dry deposition. However, measurements reported alongside accompanying meteorological and phenological parameters (e.g., LAI) could allow for a much more detailed exploration of the sources of bias in models.

Dry deposition is a globally important sink of ozone, and improving our understanding of this process will lead to improvements in the simulation of modern air quality, in the understanding of ozone damage to vegetation, and in the projected response of atmospheric composition to changes in climate and land cover.

Acknowledgments
This work was supported by National Science Foundation (ATM-1564495). The authors would like to thank Lyatt Jaeglé for useful discussions. The data used in this work are listed in the references and Table 2 and are available on request from the authors. We gratefully acknowledge the efforts of all the measurement teams behind the observations cited here.

References

Bey, I., Jacob, D. J., Yantosca, R. M., Logan, J. A., Field, B. D., Fiore, A. M., … Schultz, M. G. (2001). Global modeling of tropospheric chemistry with assimilated meteorology: Model description and evaluation. *Journal of Geophysical Research*, *106*(D19), 23,073–23,095. https://doi.org/10.1029/2001JD000807

Cape, J. N., Hamilton, R., & Heal, M. R. (2009). Reactive uptake of ozone at simulated leaf surfaces: Implications for 'non-stomatal' ozone flux. *Atmospheric Environment, Air Pollution Related to Transport*, *43*(5), 1116–1123. https://doi.org/10.1016/j.atmosenv.2008.11.007

Clifton, O. E., Fiore, A. M., Munger, J. W., Malyshev, S., Horowitz, L. W., Shevliakova, E., … Griffin, K. L. (2016). Interannual variability in ozone removal by a temperate deciduous forest. *Geophysical Research Letters*, *44*, 542–552. https://doi.org/10.1002/2016GL070923

Coe, H., Gallagher, M. W., Choularton, T. W., & Dore, C. (1995). Canopy scale measurements of stomatal and cuticular 03 uptake by Sitka spruce. *Atmospheric Environment*, *29*(12), 1413–1423. https://doi.org/10.1016/1352-2310(95)00034-V

Coyle, M., Nemitz, E., Storeton-West, R., Fowler, D., & Neil Cape, J. (2009). Measurements of ozone deposition to a potato canopy. *Agricultural and Forest Meteorology*, *149*(3-4), 655–666. https://doi.org/10.1016/j.agrformet.2008.10.020

Droppo, J. G. (1985). Concurrent measurements of ozone dry deposition using Eddy correlation and profile flux methods. *Journal of Geophysical Research*, *90*(D1), 2111–2118. https://doi.org/10.1029/JD090iD01p02111

Emberson, L. D., Kitwiroon, N., Beevers, S., Büker, P., & Cinderby, S. (2013). Scorched Earth: How will changes in the strength of the vegetation sink to ozone deposition affect human health and ecosystems? *Atmospheric Chemistry and Physics*, *13*(14), 6741–6755. https://doi.org/10.5194/acp-13-6741-2013

Fan, S.-M., Wofsy, S. C., Bakwin, P. S., Jacob, D. J., & Fitzjarrald, D. R. (1990). Atmosphere-biosphere exchange of CO2 and O3 in the Central Amazon Forest. *Journal of Geophysical Research*, *95*(D10), 16,851–16,864. https://doi.org/10.1029/JD095iD10p16851

Fang, H., Jiang, C., Li, W., Wei, S., Baret, F., Chen, J. M., … Zhu, Z. (2013). Characterization and intercomparison of global moderate resolution leaf area index (LAI) products: Analysis of climatologies and theoretical uncertainties. *Journal of Geophysical Research: Biogeosciences*, *118*, 529–548. https://doi.org/10.1002/jgrg.20051

Fares, S., McKay, M., Holzinger, R., & Goldstein, A. H. (2010). Ozone fluxes in a Pinus Ponderosa ecosystem are dominated by non-stomatal processes: Evidence from long-term continuous measurements. *Agricultural and Forest Meteorology*, *150*(3), 420–431. https://doi.org/10.1016/j.agrformet.2010.01.007

Fares, S., Weber, R., Park, J.-H., Gentner, D., Karlik, J., & Goldstein, A. H. (2012). Ozone deposition to an orange orchard: Partitioning between stomatal and non-stomatal sinks. *Environmental Pollution*, *169*, 258–266. https://doi.org/10.1016/j.envpol.2012.01.030

Finkelstein, P. L., Ellestad, T. G., Clarke, J. F., Meyers, T. P., Schwede, D. B., Hebert, E. O., & Neal, J. A. (2000). Ozone and sulfur dioxide dry deposition to forests: Observations and model evaluation. *Journal of Geophysical Research*, *105*, 15,365–15,377. https://doi.org/10.1029/2000JD900185

Fowler, D., Flechard, C., Neil Cape, J., Storeton-West, R. L., & Coyle, M. (2001). Measurements of ozone deposition to vegetation quantifying the flux, the stomatal and non-stomatal components. *Water, Air, and Soil Pollution*, *130*(1/4), 63–74. https://doi.org/10.1023/A:1012243317471

Fowler, D., Nemitz, E., Misztal, P., Di Marco, C., Skiba, U., Ryder, J., … Hewitt, C. N. (2011). Effects of land use on surface-atmosphere exchanges of trace gases and energy in Borneo: Comparing fluxes over oil palm plantations and a rainforest. *Philosophical Transactions of the Royal Society, B: Biological Sciences*, *366*(1582), 3196–3209. https://doi.org/10.1098/rstb.2011.0055

Ganzeveld, L., Helmig, D., Fairall, C. W., Hare, J., & Pozzer, A. (2009). Atmosphere-ocean ozone exchange: A global modeling study of biogeochemical, atmospheric, and waterside turbulence dependencies. *Global Biogeochemical Cycles*, *23*, GB4021. https://doi.org/10.1029/2008GB003301

Gao, W., & Wesely, M. L. (1995). Modeling gaseous dry deposition over regional scales with satellite observations—I. Model development. *Atmospheric Environment*, *29*(6), 727–737. https://doi.org/10.1016/1352-2310(94)00284-R

Geddes, J. A., Heald, C. L., Silva, S. J., & Martin, R. V. (2016). Land cover change impacts on atmospheric chemistry: Simulating projected large-scale tree mortality in the United States. *Atmospheric Chemistry and Physics*, *16*(4), 2323–2340. https://doi.org/10.5194/acp-16-2323-2016

Granat, L., & Richter, A. (1995). Dry deposition to pine of sulphur dioxide and ozone at low concentration. *Atmospheric Environment*, *29*(14), 1677–1683. https://doi.org/10.1016/1352-2310(95)00036-X

Hardacre, C., Wild, O., & Emberson, L. (2015). An evaluation of ozone dry deposition in global scale chemistry climate models. *Atmospheric Chemistry and Physics*, *15*(11), 6419–6436. https://doi.org/10.5194/acp-15-6419-2015

Heald, C. L., & Geddes, J. A. (2016). The impact of historical land use change from 1850 to 2000 on secondary particulate matter and ozone. *Atmospheric Chemistry and Physics*, *16*(23), 14,997–15,010. https://doi.org/10.5194/acp-16-14997-2016

Hole, L. R., Semb, A., & Tørseth, K. (2004). Ozone deposition to a temperate coniferous forest in Norway; gradient method measurements and comparison with the EMEP deposition module. *Atmospheric Environment*, *38*(15), 2217–2223. https://doi.org/10.1016/j.atmosenv.2003.11.042

Jacob, D. J., & Wofsy, S. C. (1990). Budgets of reactive nitrogen, hydrocarbons, and ozone over the Amazon Forest during the wet season. *Journal of Geophysical Research*, *95*(D10), 16,737–16,754. https://doi.org/10.1029/JD095iD10p16737

Kavassalis, S. C., & Murphy, J. G. (2017). Understanding ozone-meteorology correlations: A role for dry deposition. *Geophysical Research Letters*, *44*, 2922–2931. https://doi.org/10.1002/2016GL071791

Kumar, A., Chen, F., Niyogi, D., Alfieri, J. G., Ek, M., & Mitchell, K. (2011). Evaluation of a photosynthesis-based canopy resistance formulation in the Noah land-surface model. *Boundary Layer Meteorology*, *138*(2), 263–284. https://doi.org/10.1007/s10546-010-9559-z

Kurpius, M. R., McKay, M., & Goldstein, A. H. (2002). Annual ozone deposition to a Sierra Nevada Ponderosa pine plantation. *Atmospheric Environment*, *36*(28), 4503–4515. https://doi.org/10.1016/S1352-2310(02)00423-5

Lamaud, E., Brunet, Y., Labatut, A., Lopez, A., Fontan, J., & Druilhet, A. (1994). The Landes experiment: Biosphere-atmosphere exchanges of ozone and aerosol particles above a pine forest. *Journal of Geophysical Research*, *99*(D8), 16,511–16,521. https://doi.org/10.1029/94JD00668

Lawrence, D. M., Oleson, K. W., Flanner, M. G., Thornton, P. E., Swenson, S. C., Lawrence, P. J., … Slater, A. G. (2011). Parameterization improvements and functional and structural advances in version 4 of the community land model. *Journal of Advances in Modeling Earth Systems*, *3*(3) M03001. https://doi.org/10.1029/2011MS000045

Lelieveld, J., & Dentener, F. J. (2000). What controls tropospheric ozone? *Journal of Geophysical Research*, *105*(D3), 3531–3551. https://doi.org/10.1029/1999JD901011

Lin, M., Horowitz, W., Payton, R., Fiore, A. M., & Tonnesen, G. (2017). US surface ozone trends and extremes from 1980 to 2014: Quantifying the roles of rising Asian emissions, domestic controls, wildfires, and climate. *Atmospheric Chemistry and Physics*, *17*(4), 2943–2970. https://doi.org/10.5194/acp-17-2943-2017

Luhar, A. K., Galbally, I. E., Woodhouse, M. T., & Thatcher, M. (2016). An improved parameterisation of ozone dry deposition to the ocean and its impact in a global climate-chemistry model. *Atmospheric Chemistry and Physics Discussions*, *2016*, 1–40. https://doi.org/10.5194/acp-2016-844

Mao, J., Paulot, F., Jacob, D. J., Cohen, R. C., Crounse, J. D., Wennberg, P. O., … Horowitz, L. W. (2013). Ozone and organic nitrates over the eastern United States: Sensitivity to isoprene chemistry. *Journal of Geophysical Research: Atmospheres*, *118*, 11,256–11,268. https://doi.org/10.1002/jgrd.50817

Meyers, T. P., Finkelstein, P., Clarke, J., Ellestad, T. G., & Sims, P. F. (1998). A multilayer model for inferring dry deposition using standard meteorological measurements. *Journal of Geophysical Research*, *103*(D17), 22,645–22,661. https://doi.org/10.1029/98JD01564

Mikkelsen, T. N., Ro-Poulsen, H., Hovmand, M. F., Jensen, N. O., Pilegaard, K., & Egeløv, A. H. (2004). Five-year measurements of ozone fluxes to a Danish Norway spruce canopy. *Atmospheric Environment: New methods of risk assessment for ozone impacts on vegetation*, *38*(15), 2361–2371. https://doi.org/10.1016/j.atmosenv.2003.12.036

Mikkelsen, T. N., Ro-Poulsen, H., Pilegaard, K., Hovmand, M. F., Jensen, N. O., Christensen, C. S., & Hummelshoej, P. (2000). Ozone uptake by an evergreen forest canopy: Temporal variation and possible mechanisms. *Environmental Pollution*, *109*(3), 423–429. https://doi.org/10.1016/S0269-7491(00)00045-2

Muller, J. B. A., Percival, C. J., Gallagher, M. W., Fowler, D., Coyle, M., & Nemitz, E. (2010). Sources of uncertainty in Eddy covariance ozone flux measurements made by dry chemiluminescence fast response analysers. *Atmospheric Measurement Techniques*, *3*(1), 163–176. https://doi.org/10.5194/amt-3-163-2010

Munger, J. W., Wofsy, S. C., Bakwin, P. S., Fan, S.-M., Goulden, M. L., Daube, B. C., … Fitzjarrald, D. R. (1996). Atmospheric deposition of reactive nitrogen oxides and ozone in a temperate deciduous forest and a subarctic woodland: 1. Measurements and mechanisms. *Journal of Geophysical Research*, *101*(D7), 12,639–12,657. https://doi.org/10.1029/96JD00230

Munger, W., & Wofsy, S. (1999a). Concentrations and surface exchange of air pollutants at Harvard Forest EMS tower since 1990. Harvard Forest Data Archive: HF066.

Munger, W., & Wofsy, S. (1999b). Biomass inventories at Harvard Forest EMS tower since 1993. Harvard Forest data archive: HF069.

Niyogi, D. S., Raman, S., & Alapaty, K. (1998). Comparison of four different stomatal resistance schemes using FIFE data. Part II: Analysis of terrestrial biospheric-atmospheric interactions. *Journal of Applied Meteorology*, *37*(10), 1301–1320. https://doi.org/10.1175/1520-0450(1998)037%3C1301:COFDSR%3E2.0.CO;2

Padro, J., Den Hartog, G., & Neumann, H. H. (1991). An investigation of the ADOM dry deposition module using summertime O3 measurements above a deciduous forest. *Atmospheric Environment. Part A. General Topics*, *25*(8), 1689–1704. https://doi.org/10.1016/0960-1686(91)90027-5

Padro, J., Massman, W. J., Shaw, R. H., Delany, A., & Oncley, S. P. (1994). A comparison of some aerodynamic resistance methods using measurements over cotton and grass from the 1991 California ozone deposition experiment. *Boundary Layer Meteorology*, *71*(4), 327–339. https://doi.org/10.1007/BF00712174

Padro, J., Neumann, H. H., & Den Hartog, G. (1992). Modelled and observed dry deposition velocity of O3 above a deciduous forest in the winter. *Atmospheric Environment. Part A. General Topics*, *26*(5), 775–784. https://doi.org/10.1016/0960-1686(92)90237-F

Park, R. J., Hong, S. K., Kwon, H.-A., Kim, S., Guenther, A., Woo, J.-H., & Loughner, C. P. (2014). An evaluation of ozone dry deposition simulations in East Asia. *Atmospheric Chemistry and Physics*, *14*(15), 7929–7940. https://doi.org/10.5194/acp-14-7929-2014

Parrella, J. P., Jacob, D. J., Liang, Q., Zhang, Y., Mickley, L. J., Miller, B., … van Roozendael, M. (2012). Tropospheric bromine chemistry: Implications for present and pre-industrial ozone and mercury. *Atmospheric Chemistry and Physics*, *12*(15), 6723–6740. https://doi.org/10.5194/acp-12-6723-2012

Pilegaard, K., HummelshØj, P., & Jensen, N. O. (1998). Fluxes of ozone and nitrogen dioxide measured by Eddt correlation over a harvested wheat field. *Atmospheric Environment*, *32*(7), 1167–1177. https://doi.org/10.1016/S1352-2310(97)00194-5

Pio, C. A., Feliciano, M. S., Vermeulen, A. T., & Sousa, E. C. (2000). Seasonal variability of ozone dry deposition under Southern European climate conditions, in Portugal. *Atmospheric Environment*, *34*(2), 195–205. https://doi.org/10.1016/S1352-2310(99)00276-9

Rummel, U., Ammann, C., Kirkman, G. A., Moura, M. A. L., Foken, T., Andreae, M. O., & Meixner, F. X. (2007). Seasonal variation of ozone deposition to a tropical rain forest in Southwest Amazonia. *Atmospheric Chemistry and Physics*, *7*(20), 5415–5435. https://doi.org/10.5194/acp-7-5415-2007

Sadiq, M., Tai, A. P. K., Lombardozzi, D., & Martin, M. V. (2017). Effects of ozone-vegetation coupling on surface ozone air quality via biogeochemical and meteorological feedbacks. *Atmospheric Chemistry and Physics*, *17*(4), 3055–3066. https://doi.org/10.5194/acp-17-3055-2017

Schwede, D., Leiming, Z., Robert, V., & Gary, L. (2011). An intercomparison of the deposition models used in the CASTNET and CAPMoN networks. *Atmospheric Environment*, *45*, 1337–1346. https://doi.org/10.1016/j.atmosenv.2010.11.050

Sigler, J. M., Fuentes, J. D., Heitz, R. C., Garstang, M., & Fisch, G. (2002). Ozone dynamics and deposition processes at a deforested site in the Amazon Basin. *Ambio: A Journal of the Human Environment*, *31*(1), 21–27. https://doi.org/10.1579/0044-7447-31.1.21

Silva, S. J., Heald, C. L., Geddes, J. A., Austin, K. G., Kasibhatla, P. S., & Marlier, M. E. (2016). Impacts of current and projected oil palm plantation expansion on air quality over Southeast Asia. *Atmospheric Chemistry and Physics*, *16*(16), 10,621–10,635. https://doi.org/10.5194/acp-16-10621-2016

Stella, P., Personne, E., Loubet, B., Lamaud, E., Ceschia, E., Béziat, P., … Cellier, P. (2011). Predicting and partitioning ozone fluxes to maize crops from sowing to harvest: The Surfatm-O3 model. *Biogeosciences*, *8*(10), 2869–2886. https://doi.org/10.5194/bg-8-2869-2011

Travis, K. R., Jacob, D. J., Fisher, J. A., Kim, P. S., Marais, E. A., Zhu, L., … Zhou, X. (2016). Why do models overestimate surface ozone in the Southeast United States? *Atmospheric Chemistry and Physics*, *16*(21), 13,561–13,577. https://doi.org/10.5194/acp-16-13561-2016

Turnipseed, A. A., Burns, S. P., Moore, D. J. P., Hu, J., Guenther, A. B., & Monson, R. K. (2009). Controls over ozone deposition to a high elevation subalpine forest. *Agricultural and Forest Meteorology*, *149*(9), 1447–1459. https://doi.org/10.1016/j.agrformet.2009.04.001

van der Werf, G. R., Randerson, J. T., Giglio, L., Collatz, G. J., Mu, M., Kasibhatla, P. S., … van Leeuwen, T. T. (2010). Global fire emissions and the contribution of deforestation, savanna, forest, agricultural, and peat fires (1997–2009). *Atmospheric Chemistry and Physics*, *10*(23), 11,707–11,735. https://doi.org/10.5194/acp-10-11707-2010

Wang, Y., Jacob, D. J., & Logan, J. A. (1998). Global simulation of tropospheric O3-NO X -hydrocarbon chemistry: 3. Origin of tropospheric ozone and effects of nonmethane hydrocarbons. *Journal of Geophysical Research*, *103*(D9), 10,757–10,767. https://doi.org/10.1029/98JD00156

Wesely, M. L. (1989). Parameterization of surface resistances to gaseous dry deposition in regional-scale numerical models. *Atmospheric Environment*, *23*(6), 1293–1304. https://doi.org/10.1016/0004-6981(89)90153-4

Wesely, M. L., & Hicks, B. B. (2000). A review of the current status of knowledge on dry deposition. *Atmospheric Environment*, *34*(12-14), 2261–2282. https://doi.org/10.1016/S1352-2310(99)00467-7

Wu, Y., Brashers, B., Finkelstein, P. L., & Pleim, J. E. (2003). A multilayer biochemical dry deposition model. 1. Model formulation. *Journal of Geophysical Research*, *108*(D1), 4013. https://doi.org/10.1029/2002JD002293

Wu, Z., Wang, X., Chen, F., Turnipseed, A. A., Guenther, A. B., Niyogi, D., … Alapaty, K. (2011). Evaluating the calculated dry deposition velocities of reactive nitrogen oxides and ozone from two community models over a temperate deciduous forest. *Atmospheric Environment*, *45*(16), 2663–2674. https://doi.org/10.1016/j.atmosenv.2011.02.063

Yu, S., Eder, B., Dennis, R., Chu, S.-H., & Schwartz, S. E. (2006). New unbiased symmetric metrics for evaluation of air quality models. *Atmospheric Science Letters*, *7*(1), 26–34. https://doi.org/10.1002/asl.125

Zhang, L., Brook, J. R., & Vet, R. (2002). On ozone dry deposition—With emphasis on non-stomatal uptake and wet canopies. *Atmospheric Environment*, *36*(30), 4787–4799. https://doi.org/10.1016/S1352-2310(02)00567-8

Zhang, L., Brook, J. R., & Vet, R. (2003). A revised parameterization for gaseous dry deposition in air-quality models. *Atmospheric Chemistry and Physics*, *3*(6), 2067–2082. https://doi.org/10.5194/acp-3-2067-2003

Zhou, P., Ganzeveld, L., Rannik, Ü., Zhou, L., Gierens, R., Taipale, D., … Boy, M. (2017). Simulating ozone dry deposition at a boreal forest with a multi-layer canopy deposition model. *Atmospheric Chemistry and Physics*, *17*(2), 1361–1379. https://doi.org/10.5194/acp-17-1361-2017